Engineered Science
DOI: https://dx.doi.org/10.30919/es1704

Wireless Ammonia Gas Sensor based on P-type Porous Si: Methods, Materials and Design

Alisher Skabylov,[1] Lazzat Abdizhalilova,[1] Margulan Ibraimov,[1] Bakyt Khaniyev,[1] Yerbolat Tezekbay[1,2,*] Muhammad Abdullah,[2] Raikhan Azamat,[1] Olzat Toktarbaiuly[2,*] and Tolagay Duisebayev[1,2,*]

Abstract

This study investigates the 4S performance parameters (selectivity, sensitivity, stability, speed) of a porous silicon (PS)-based gas sensor and develops a portable, wireless electronic device for ammonia detection. The porous silicon layer was fabricated by electrochemically etching p-type (100) crystalline silicon using a hydrofluoric acid (HF) and ethoxyethanol electrolyte in a 1:2 volume ratio. A compact sensor module was developed, integrating a comparator circuit, Wi-Fi connectivity, a web-based monitoring platform, and the PS sensing element, fabricated using a ProtoMat E44 CNC plotter and housed in a 3D-printed PLA enclosure. The optimized sensor exhibited a high sensitivity of 42% to ammonia, surpassing responses to other gases. The system leverages an ESP32 microcontroller for real-time data acquisition, enabling remote monitoring via a custom IoT platform with email/SMS alerts for gas concentration thresholds. The results validate the feasibility of room-temperature operation, eliminating the need for heating elements while maintaining rapid response (20 s) and stability over 10 days. This work advances the development of low-power, portable gas sensors for environmental and industrial safety applications.

Keywords: Neurotoxicity, Hepatotoxicity, Environmental Impact, Human Health, Livestock.
Received: 10 June 2025; Revised: 13 August 2025; Accepted: 22 August 2025
Article Type: Research article.

1. Introduction

Modern gas detection technologies are crucial for safety and environmental protection. The development of portable electronic gas sensors based on semiconductor nanostructured films significantly contributes to this field by enabling the efficient detection of harmful gases under various operating conditions. Numerous gas sensors are available on the market; each tailored to specific applications and offering unique advantages. Nevertheless, the need for high sensitivity, rapid response time, low power consumption, and affordability remains crucial for advancing this field.

In the context of these requirements, sensors based on porous silicon show significant superiority due to their compatibility with silicon technologies.[1] Earlier work with simple Schottky-contacted Al/p-Si/Al structures validated the effectiveness of silicon-based platforms for ammonia detection, reporting fast response and operation at ambient temperatures.[2] Such systems paved the way for today's more complex nanostructured porous silicon sensors. Porous silicon has a tunable morphology as well as unique electrical and optical properties, which extends its application as an active material for gas sensors. Black silicon hyperdoped with aluminum has emerged as a promising substrate for ammonia gas sensing, combining enhanced carrier mobility and surface reactivity. Li *et al.* showed improved sensor response, selectivity, and long-term durability at room temperature using this approach.[3] The step-bunched silicon morphology,[4,5] used as a substrate for thin films and nanowires, has also been extensively studied by researchers due to its influence on sensor performance. Recent studies have shown that porous SnO_2 nanosheets can detect ammonia at ultralow concentrations (~64 ppt) and with rapid response (~8 seconds), even under extreme humidity, emphasizing the potential of porous nanomaterials in variable environmental conditions.[6] By utilizing the optical parameters of the material, the influence of electrical noise can be reduced, which in turn improves the accuracy and reliability of measurements. Recent innovations in laser-induced graphene (LIG)

[1]*Department of Physics and Technology, Al-Farabi Kazakh National University, Almaty, 050040, Kazakhstan*
[2]*Renewable Energy Laboratory, National Laboratory Astana (NLA), Nazarbayev University, 53 Kabanbay Batyr Astana, 010000, Kazakhstan*
[*]*Email:* tolagay.duisebayev@nu.edu.kz (T. Duisebayev), olzat.toktarbaiuly@nu.edu.kz (O. Toktarbaiuly)

technology have enabled the development of highly responsive room-temperature ammonia sensors. Santos-Ceballos *et al*. demonstrated that polyaniline-coated LIG structures exhibit strong ammonia selectivity, a response time under 15 seconds, and operability under ambient conditions without heating elements.[7] In particular, the design of the Rugate filter – an optical filter that reflects certain wavelengths due to changing refractive index incrementally – can be used to amplify the fluorescence signal that registers the changes occurring during the interaction of the material with gas.[8]

There are various approaches to recording changes in electrical parameters and fluorescence during optical sensing, which allows effective tracking of material-gas interactions. In one of the studies, the potential difference (photo-EMF) through contacts located on the bottom and top layers of porous silicon was measured when the samples were illuminated.[9] The results showed that increasing the concentration of ammonia in the measuring chamber leads to a decrease in the photo-EMF value. Nevertheless, the most common and convenient method remains the detection of changes occurring in the electrical properties of the material when it interacts with gas. Similarly, rGO/SnO_2 nanocomposite-based ammonia sensors have demonstrated fast response, high selectivity, and self-powered operation at room temperature, making them ideal for autonomous environmental sensing applications.[10]

In addition, the process of porous silicon formation also affects gas detection methods. For example, the development of algorithms that ensure stable and high fluorescence, as well as the design of an electrode capable of fast reaction times, are important aspects. The efficient utilization of heterostructures also opens new horizons in the development of gas sensors. In particular, the modification of porous silicon surface with copper oxide (CuO) and tin dioxide (SnO_2) by laser firing at an intensity of 40 mW/cm^2 showed that the nanocomposite with a ratio of 70% SnO_2:30% CuO has the best sensitivity to ammonia, reaching 88%.[11-15] Recent research on GaN synthesis via plasma-enhanced chemical vapor deposition has also highlighted the material's potential for optoelectronic integration, showing how substrate properties and doping ratios influence performance in photoactive applications such as dye-sensitized solar cells.[16]

The novelty of this work lies in the complete integration of a PS-based sensing element with a compact, wireless IoT-enabled system, housed in a 3D-printed PLA enclosure. Unlike many existing designs, our sensor operates entirely at room temperature, features a fast electrical response (~20 s), and allows real-time data transmission using an ESP32-based system. This configuration enables portable, long-term environmental monitoring without the need for external heating or large power sources, filling a critical gap between material innovation and device-level application. The integration of microcontrollers and wireless modules to enable remote communication with the sensor is also an important aspect. Wireless-enabled ammonia sensors have also progressed significantly. A recent study reported a flexible PANI/MWCNT-based sensor integrated with Wi-Fi modules, capable of detecting ammonia concentrations down to 0.3 ppm in real time via cloud-connected platforms.[17] The system operated at room temperature, enabling wearable and portable environmental monitoring. The choice of communication technologies depends on distance, radius covered, functionality, and data rate. Mobile communication technologies (GSM) are preferred for remote control in remote areas.[18,19] At distances of up to one hundred meters, especially in indoor environments, high-speed Wi-Fi and ZigBee technologies provide reliable connectivity, with ZigBee offering greater data and software sharing capabilities.[20] In the context of controlling and monitoring a handheld device, Bluetooth is the preferred technology to provide the necessary range of operation.[21-24]

Despite recent progress in ammonia vapor sensors, there remains a gap in the detailed documentation of production parameters and real-time integration for portable, low-power systems. In this study, we hypothesize that a porous silicon-based ammonia sensor, integrated with a compact, wireless IoT platform, can provide fast response, high selectivity, and stable performance at room temperature without requiring external heating. The primary goal of this work is to develop and validate a portable, low-cost electronic gas sensor based on porous silicon, optimized for wireless ammonia detection under ambient conditions, with industrial applicability.

2. Materials and methods - Design and manufacture of gas sensor module

2.1 Sensitive element of the sensor

The electrochemical etching process, as described in previous studies,[25] was used to fabricate the sensor sensing element. Before etching, the substrates were cleaned using a standard method involving ethanol and acetone in an ultrasonic bath.[26] Porous silicon (PS) samples were fabricated from p-type boron-doped crystalline silicon (c-Si) wafers with an orientation of (100) and a resistivity of 10 Ohm-cm. The anodization was performed on 21 mm × 21 mm wafers using an electrolyte composed of hydrofluoric acid (40%) and ethoxyethanol in a 1:2 volume ratio (there is one 1:1 HF:$C_4H_{10}O_2$ based film (№9) and one HF: Acetonitrile film (№8)). Several experiments were performed to determine the effective parameters for the creation of nanostructures, after which the samples were washed with water and dried in air. Excessively low current densities result in pore sizes that are insufficient for effective gas sensing, while excessively high current densities reduce nanocrystal dimensions. Although higher currents may produce a larger specific surface area, they often lead to structural anomalies and instability. Therefore, medium-range current densities are considered optimal for fabricating porous silicon films with favorable propertie.[34] The values of current density, etching time, and applied voltage selected for the fabrication process, as presented in Table 1, were established through two rounds of

Table 1: Electrochemical etching parameters of two-dimensional porous silicon samples.

Experiment	Current density, mA/ cm^2	Voltage, V	Etching time, min
1	12	9	8
2	12	9	45
3	17	12	30
4	20	17	30
5	30	25	20
6	40	30	15
7	50	40	4
8	20	17	30
9	5	30	40

experimental validation for each parameter. The voltametric response was measured to evaluate the electrical characteristics. A GaIn alloy ohmic contact was placed on the surface of the film to establish the electronic coupling used for electrical characterization. The production parameters were determined through the time dependence of current intensity, which allowed the determination of effective parameters for gas detection in porous silicon films, which serve as the sensitive element of the sensor obtained at different current densities.

2.2 Manufacturing of gas sensor module

To realize the sensing element created in the experiment as a gas sensor in electronic devices, an electrical circuit including advanced components has been developed. In this paper, a gas sensor electrical module was developed that differs from traditional solutions, such as MQ sensors, in that it operates at room temperature, which eliminates the need for additional heating and increases the energy efficiency of the device. This is particularly important in applications where gas concentrations are constantly monitored, as the reduced power consumption contributes to longer device operation without the need for frequent recharging.

To realize the circuit, an LPKF Protomat E44 plotter was used to create the printed circuit board, ensuring a highly accurate and compact design. The body of the device was printed on a 3D printer, which not only improves ergonomics but also allows the design to be quickly customized to meet specific requirements. The use of additive technology in the production of device components significantly reduces prototyping time and increases design flexibility.

2.3 Electronic gas sensor

The electronic gas sensor is based on the ESP32 microcontroller, which was chosen for its Wi-Fi integration capabilities and sufficient processing power to handle data from multiple sensors. The combined use of the mentioned microcontroller and the Firebase platform enables the efficient implementation of smart home automation.[31] This allows the device to send gas sensor status notifications to email or smartphone, making it user-friendly. Compared to smaller microcontrollers such as the Arduino Pro Mini and Wemos D1 Mini, the ESP32 offers significant advantages, as it features a built-in Wi-Fi module and does not require additional external components.[32] Thanks to its dual-core processor and wireless communication capabilities, data processing is faster, and energy consumption is lower, making it a suitable solution for real-time data synchronization and cloud-based control in IoT applications and for wearable devices.[33] This allows the device to send gas sensor status notifications to email or smartphone, making it user-friendly. In addition to the gas sensor, the device includes temperature and humidity sensors, as well as a motion sensor and SD card to expand its functionality.

The electronic device includes:

- ESP32 microcontroller - provides wireless communication via Wi-Fi and has enough processing power to handle data from multiple sensors.
- Gas sensor module - responsible for detecting gas concentrations and transmitting data to the system.
- Temperature and humidity sensor - for environmental monitoring. Temperature and humidity sensing is important because these parameters can significantly affect the measurement accuracy of a gas sensor. For example, the concentration of some gases can vary with temperature and humidity, which must be considered for proper interpretation of the data. Built-in temperature and humidity sensors allow the device to automatically correct its readings, as well as alert the user to possible measurement errors under extreme environmental conditions. This also allows you to monitor the microclimate in rooms where environmental control is important.
- Motion sensor - to detect presence in the device. The motion sensor plays a key role in improving safety when using the device in areas where continuous gas monitoring is required. It allows you to determine if there are people in the room when a gas sensor is triggered. If the gas sensor detects a leak, the motion sensor will help confirm if there are people in the room and if they remain in the danger zone, additional safety measures such as alarms or emergency alerts can be activated. This adds a layer of protection and helps to respond quickly to a threat.
- SD card - used to store sensor status data to allow further analysis and identification of patterns in changes in gases, temperature, humidity or human presence. Storing data on the SD card enables the logging of events, which is important for long-term monitoring and analysis. This allows not only tracking the dynamics of changes, but also diagnostics in case of abnormal situations. Data from the card can help to identify the causes of gas leaks and improve the monitoring system in the future.

Wiring diagram

Fig. 1 shows a schematic diagram of the device developed in EasyEDA software environment and transferred to LPKF

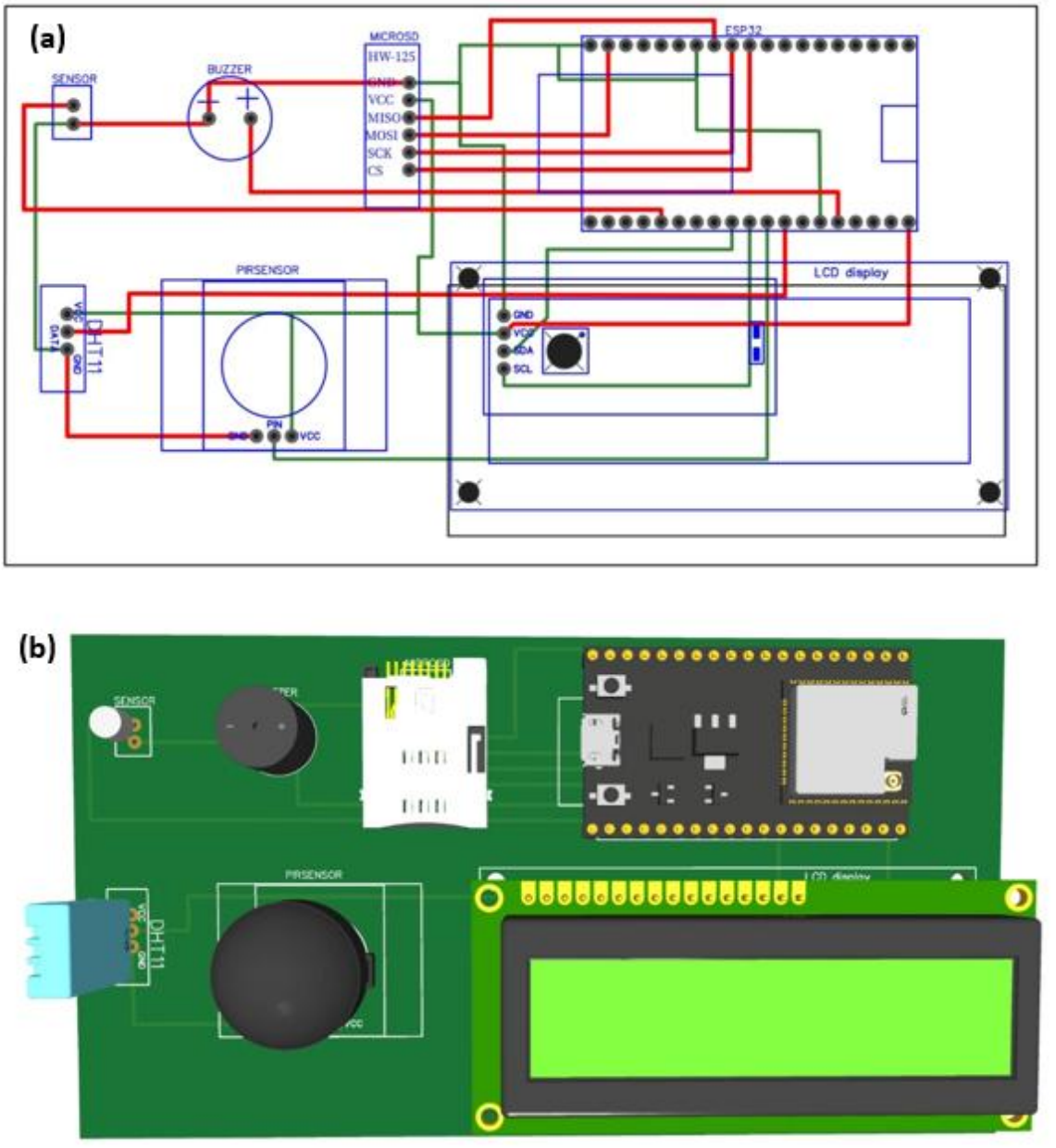

Fig. 1: Electronic sensor architecture: (a) Circuit diagram, and (b) visual model of the electronic sensor.

Protomat E44 for implementation on the PCB, as well as a 3D image of the device made in Protomat E44, which visualizes the distribution of components on the PCB.

The gas sensor is powered via the 3.3V pin of the ESP32 microcontroller, with its ground terminal linked to the ESP32's GND pin. Analog outputs from the sensors route to dedicated ESP32 input pins for analog-to-digital conversion, enabling precise data acquisition. For local data storage, an SD card interfaces with the system through the SPI protocol. Audible alerts are generated by a buzzer connected to a digital output pin, while integrated temperature and humidity sensors provide real-time environmental monitoring to enhance measurement accuracy.

Fig. 2 shows the result of the PCB design made on LPKF Protomat E44, with clearly labeled pins and connections between components.

Fig. 3 shows the 3D-printed device enclosure that provides protection and ergonomics.

The operation of the device is facilitated by an integratedWi-Fi module, which plays a central role in enabling wireless communication and real-time monitoring. Through this module, users can remotely access and observe sensor data, including both input readings and output responses, via a connected platform. This feature enhances the usability of the system by allowing continuous oversight without the need for a physical connection to the device.

In situations where gas concentrations surpass predefined safety thresholds, the system is programmed to initiate an automatic alert process. Notifications are promptly sent to the user through various channels, including email and mobile applications, ensuring timely awareness and quick response to potentially hazardous conditions. This safety mechanism adds

an important layer of protection, particularly in environments where gas leaks or accumulation could pose serious risks.

The physical structure of the prototype is enclosed in a custom-designed housing, which was fabricated using 3D printing technology. Polylactic acid (PLA) filament was selected as the printing material due to its ease of use, environmental friendliness, and mechanical stability.[30] The resulting enclosure offers a well-balanced combination of protection, ergonomics, and aesthetic appeal. It also ensures that internal components are securely held in place, minimizing the risk of damage during handling or operation.

Internally, all electronic components are neatly assembled on a custom-printed circuit board (PCB). This PCB was designed using the EasyEDA software suite, which provided a flexible and efficient platform for schematic capture and layout optimization. The finalized design was then transferred to the LPKF Protomat E44 plotter, which enabled high-precision fabrication of the circuit board. This process ensures reliable electrical connectivity, compact organization of components, and ease of integration into the final device.

3. Results and discussion

3.1 Sensor material characterization

Due to the variation of parameters due to the optical and electrical properties of porous silicon, many papers have been published for use in the field of gas sensor fabrication. In this work, it is intended to determine the presence of gas in the medium due to the change in the resistance of the material when the surface area of porous silicon interacts with gas molecules. For this purpose, the current-voltage (I–V) characteristics and sensitivity to the target gas have been studied considering the porosity of the obtained samples (Fig. 4).

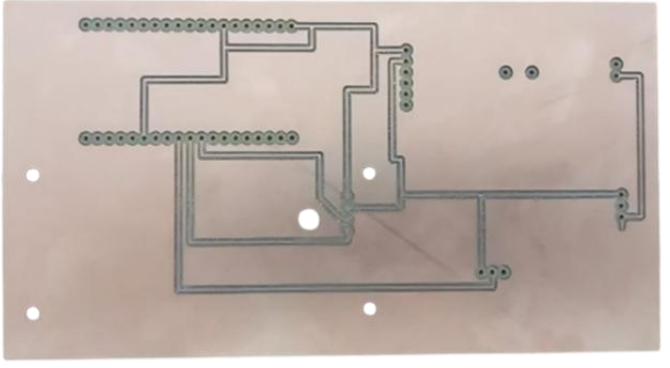

Fig. 2: Designing a printed circuit board.

We investigate the change in resistance when a voltage is applied to the material to relate it to the sensitivity index. Here, the conductive property of the limiting voltage of the semiconductor is independent of the change in current density when the films are removed in a certain sequence. That is, we cannot say that the value of current density below or above, indicating the sensitivity level that is important for the sensor, is effective. The effective parameter is at an average level.

As shown in Fig. 4, the I–V characteristics of porous silicon highlight its semiconductor properties and the impact of porosity on charge carrier mobility and gas interaction surface area. The resistance of the material, as indicated by the slope of the lines, is of great importance for the sensitivity of the sensor. The sensitivity is not only a function of current density but of an average effective parameter, consistent with Ozdemir and Gole's (2007) concern for the design of porous silicon for gas sensing.[1] The parameter is probably relevant to a balance between surface area for gas adsorption and electrical conductivity throughout the porous material, important for maximum gas sensing capability as identified by Li *et al*. (2025).[34] This equilibrium affects both electrical signal transduction and gas molecule adsorption. Therefore, the I–V behavior highlights the significance of having a best etching condition that simultaneously optimizes porosity and conductivity towards increased gas sensor sensitivity. This knowledge, as underlined by the literature cited, holds crucial bearings for porous silicon gas sensor development.

Fig. 3: Electronic device enclosure.

Since the measurement of the sample size in the crystalline state and in the porous state is determined by experiment, the accuracy of the method is low due to environmental factors. In particular, this is due to the technological difficulties of mass measurement in nanoscale volumes and removal of the porous silicon layer (gravimetric method). Accordingly, as an effective approach, it can be determined by the ratio of black pixels to the number of all pixels in the SEM image of the sample (Fig. 5).

The porosity of the samples was calculated using surface data from SEM images in the Python programming language. For this, the image is converted to grayscale utilizing the OpenCV module, and then thresholding is applied to retain only black and white pixels. Porosity is identified as the ratio of white pixels to the total number of pixels.

In Fig. 5 presented SEM images of two samples with the best sensitivity. Here as prime examples selected samples with anodization densities 12 mA/cm^2 and 17 mA/cm^2. The first sample has 36% sensitivity to ammonia gas; next one is described with stability.

According to fig. 5, by looking at the cross-section images, can see that the cross-sectional dimensions of the examples with good sensitivities are approximately the same. The

porosity of examples are equal to 52.17% and 70.46% respectively. In addition, calculated porosity of other sensors.

Fig. 6 shows the relationship between porosity and etching current density. It can be described as at average current densities, the films demonstrate excellent porosity characteristics, but for good sensitivity, it is quite sufficient to achieve porosity between 50-70 percent. The porosity maximum at intermediate current densities indicates an optimum compromise between surface area for gas interaction and structural integrity for electrical conductivity. Passage outside this range can result in compromised sensitivity through either a lack of surface area at lower porosities or interference with electrical paths at higher porosities. Overall, a porosity of the 50-70% range is key to ensuring maximum sensor sensitivity. This balance is critical to successful gas sensing, as it establishes both sufficient gas interaction and preserved electrical conductivity within the porous silicon matrix.

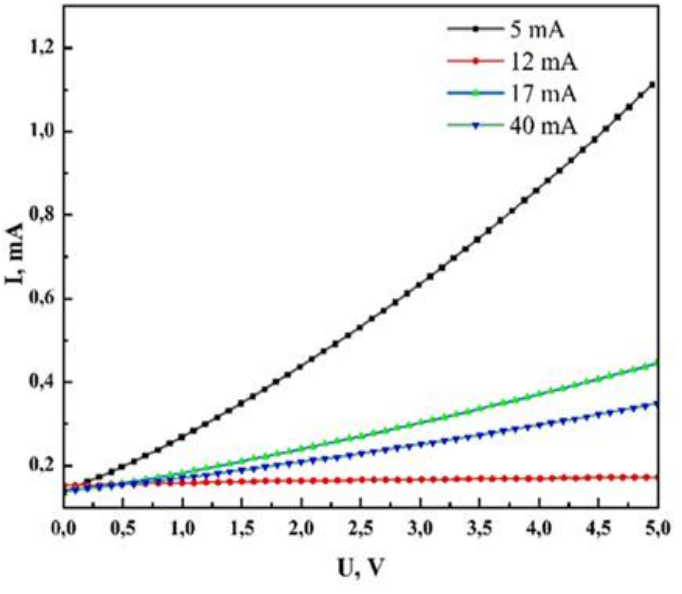

Fig. 4: Current-voltage characteristic of two-dimensional porous silicon samples.

In Fig. 7, given dependence porosity on sensitivity demonstrates the parabola in reverse, showing linear growth at the beginning. However, after 60% porosity the sensitivity decreases. Based on this data, it can be concluded that at average porosity are optimal for sensitivity. Moderate porosity (50-70%) is preferable as it gives the sensor an optimum balance between higher surface area, on which the gas adsorbs, and maintenance of electrical contactivity (percolation channels), which are needed to carry a signal. In case of low porosity, there is inadequate surface area to allow proper interaction between gas and a surface. On the other hand, at excessively high porosity, the material can be rendered devoid of a continuous conductive path, and thus a lower electrical condition will be achieved. Thus, the peak in sensitivity is caused by the tradeoffs between increased gas diffusion/adsorption and stable charge transport network.[19]

Fig. 8 shows the Raman spectrum of a porous silicon (PS) sample etched at 17 mA/cm^2. The strongest feature in the Raman spectrum of porous silicon is the Si-Si peak at about 520 cm^{-1}, corresponding to the first-order Raman scattering of the silicon crystal lattice. This peak is due to the symmetric stretching of the silicon-silicon bonds of the material and shows that the porous silicon maintains its essential crystalline structure even after etching.

The occurrence of this peak is of utmost importance since it indicates the retention of the crystallinity of the silicon matrix, albeit with nanoscale changes inherent in the electrochemical etching process. These changes are important in order to increase the gas sensing performance of the material since they control the surface area accessible to gas interaction and also the reactivity of the material.

The Raman spectrum provides crucial insights into the structural characteristics of porous silicon, confirming that the material retains its crystalline nature while exhibiting the nanoscale porosity necessary for effective gas sensing. This relative balance between porosity and crystallinity is especially important when creating high-performance gas sensors.

The observed XRD peak at 69.2° 2θ in porous silicon shown in Fig. 9, corresponds primarily to the (four hundred) diffraction plane of crystalline silicon, which typically appears at 69.1° in bulk silicon. The slight peak shift of 0.1° and broadening can be attributed to several structural modifications induced by the porosification process. First, the maintained presence of this peak indicates preserved crystallinity in the silicon matrix, though the increased full-width-at-half-maximum (FWHM) suggests reduced crystallite size due to pore formation. Second, the peak broadening may reflect the coexistence of nanocrystalline and amorphous phases resulting from disrupted long-range order. Third, potential lattice strain from the porous structure could account for the minor peak position variation. Notably, the absence of secondary peaks at ~22° or ~28° 2θ suggests minimal silicon oxide formation in these samples. The exact peak characteristics (intensity, FWHM, and position) are strongly influenced by the pore size distribution and overall porosity, as these factors modify X-ray scattering coherence. These XRD results collectively demonstrate that the porous silicon retains its fundamental crystalline structure while exhibiting nanoscale modifications characteristic electrochemical etching process.

3.2 Production parameters: 4 “S”

To evaluate the performance of a gas sensor, the main 4 “S” parameters Sensitivity, Stability, Selectivity, Speed (response/recovery rate) are taken into account.[27]

A process for estimating these parameters was developed for samples obtained at 5 мА/cm^2 см^2, 12 мА/cm^2, 17 мА/cm^2, 40 мА/cm^2 current densities. The aim here was to determine effective parameters for gas detection in porous silicon films that serve as a sensing element obtained at low, medium and

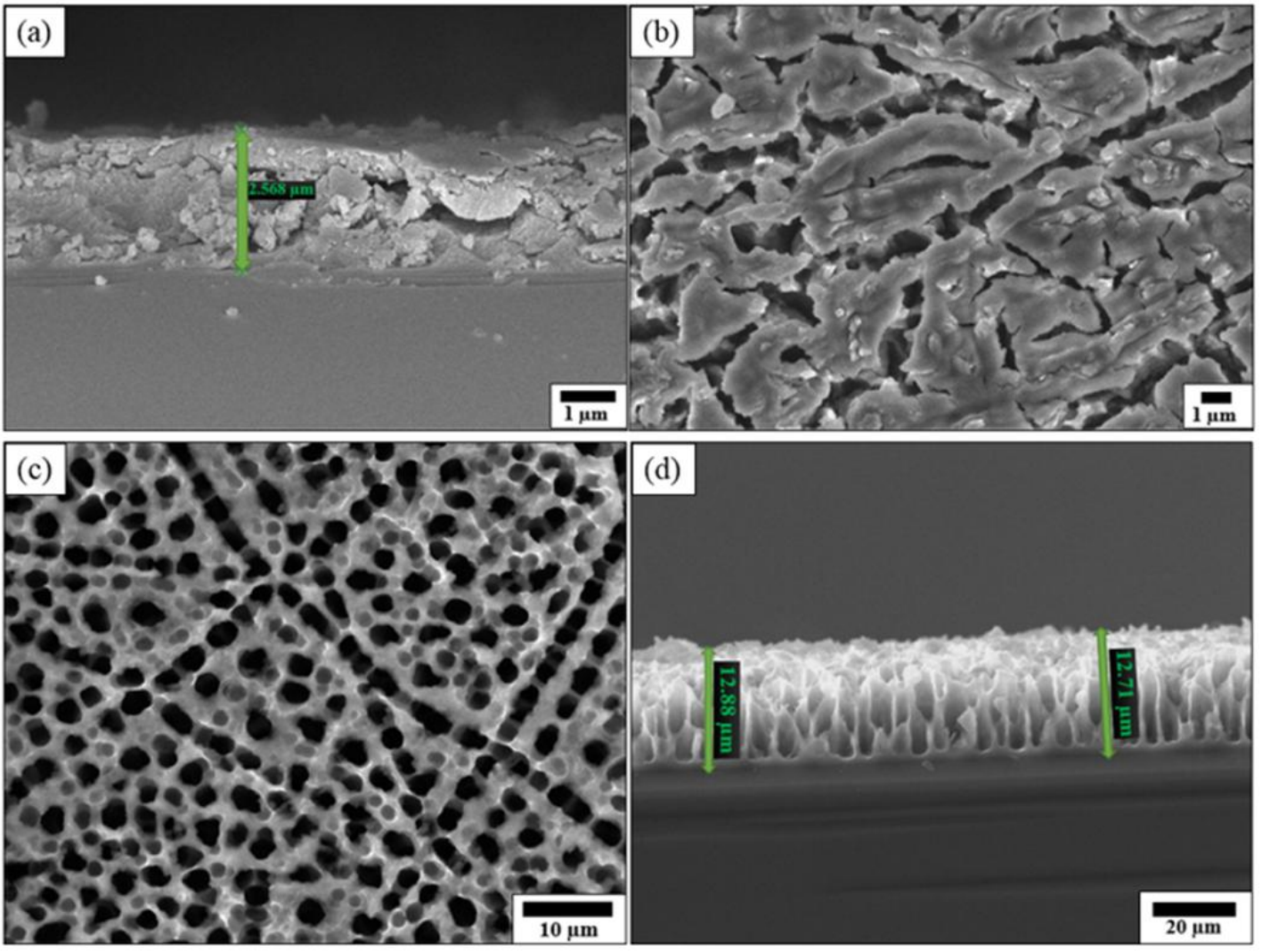

Fig. 5: SEM images of the selected samples: (a) cross-section area of the sample fabricated under 12 mA/cm^2, (b) surface of the film formed at 12 mA/cm^2, (c) top-view of the sample anodized at 17 mA/cm^2 and (d) cross-sectional morphology of the film obtained at 17 mA/cm^2.

high current densities.

Usually, the sensitivity index is calculated from the change in resistance of the material. Eq. 1.[28]

$$S = \frac{|\Delta R|}{R_0} * 100\% = \frac{|R_{gas} - R_0|}{R_0} * 100\%, \quad (1)$$

where S – sensitivity, R_{gas} – the sensor resistance in the presence of the target gas, R_0 – the baseline resistance in air.

Note that the sensitivity (S) is calculated as a relative percentage change in resistance and is not normalized to gas concentration (*e.g.*, not expressed in %/ppm). Each sensitivity value corresponds to a specific tested concentration.

From Fig. 10 (a-d), the response speed and sensitivity index of the gas sensor can be approximated when PS samples are exposed to ammonia gas. Each plot shows the variation of current (I, in mA) with time (t, in seconds) upon ammonia exposure, giving information about the dynamic behavior of the sensor.

The sensitivity and response rate of the gas sensor may be approximated from these plots. The greater the peak in the current, typically, the higher the sensitivity towards ammonia, and the slope of the curve depends on the response rate. The values calculated for sensitivity and response times are compiled in Table 2.

The findings indicate that the sample etched at 12 mA/cm^2 has the best sensitivity to ammonia with a sensitivity index of 42% and response time of around 20 seconds. This indicates that an intermediate current density achieves a best balance of surface area for gas adsorption and electrical conductivity, which is essential for sensor performance.

On the other hand, the sample etched at lower (5 mA/cm^2) and higher (40 mA/cm^2) current densities exhibit lower sensitivities and distinguishable response behavior. The sample etched at 5 mA/cm^2 exhibits a sensitivity of 12% with a quicker response time of approximately 8 seconds, whereas the sample etched at 40 mA/cm^2 exhibits a sensitivity ofmerely 6% with a response time of around 13 seconds.

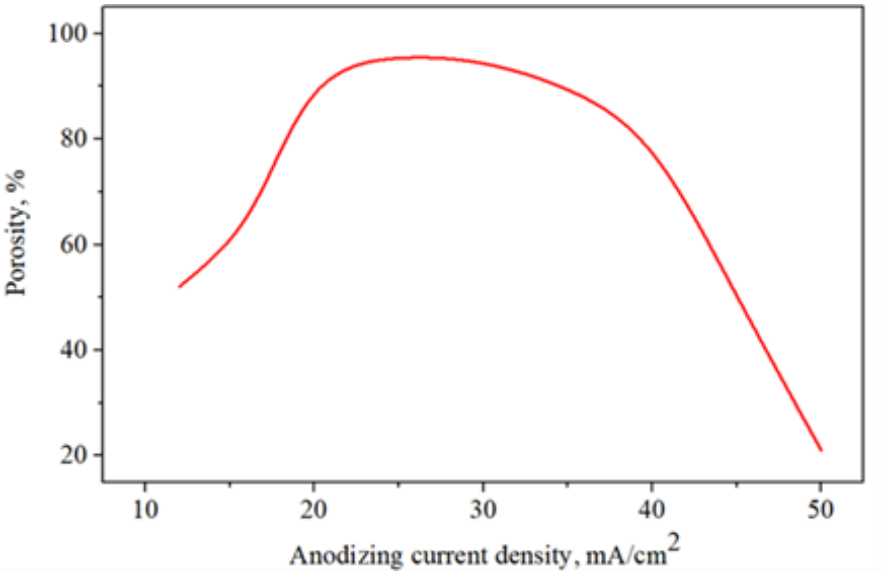

Fig. 6: Porosity as a function of current density.

These results highlight the significance of choosing the right anodizing current density to obtain the needed sensor performance. The trade-off between porosity, having an impact on the surface area exposed to the interaction with the gas, and ensuring electric conductivity in the porous material is vital to maximize sensitivity and response rate in gas sensors.

The effective model parameters were set as 12 mA/cm^2, 9V, 45 minutes, which showed a 42% change when exposed to gas vapor. The reason for our selection by sensitivity is its direct relationship with the concentration parameter, the increase of which is considered dangerous in the environment. N. Baran *et al*. established the dependence of the sensitivity index on the concentration of gas particles for gaseous ammonia.[29] According to the study, the change in sensitivity level and concentration value is approximately directly proportional.

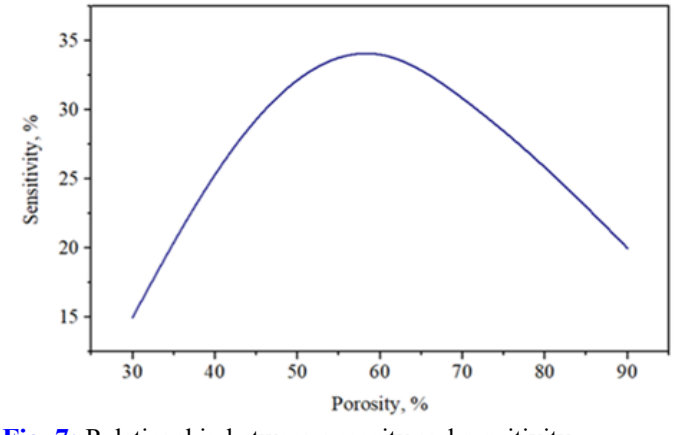

Fig. 7: Relationship between porosity and sensitivity.

In the selected sample, the stability index, considered as the next important parameter characterizing the sensor, was studied for 10 days, as other authors have done.[30] To evaluate the stability of the gas sensor, the maximum level of change in the current value under gas influence was recorded in the sample. And in programming the operation of the sensor, it is necessary stability parameters to fix the maximum value and write in the code. The stability of the PS based gas sensor shown in Fig. 11 (a) is in the range of 0.185-0.189 mA for the selected gas, with the maximum current value at the obtained time intervals.

The effect of gases such as alcohol, acetone and ammonia on the PS in Fig. 11 (b) has been studied. All measurements were performed at room temperature using vapors at an equal registering the response. The response was defined as a percentage change in the signal relative to current value in air. concentration. The sensor signal was allowed to stabilize before registering the response. The response was defined as a percentage change in the signal relative to current value in air.

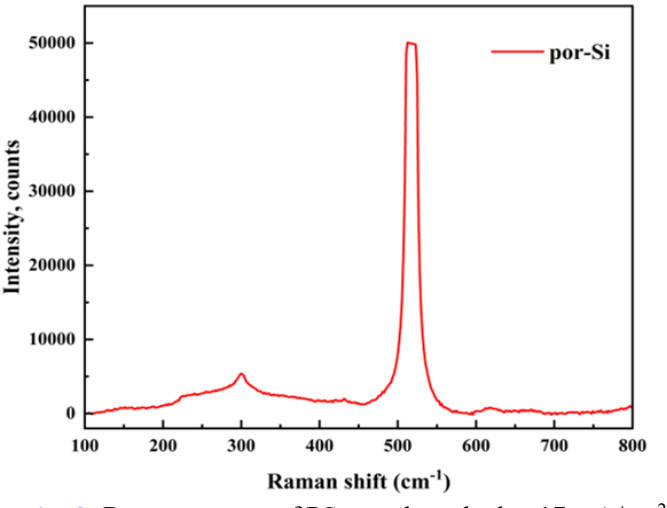

Fig. 8: Raman spectra of PS sample etched at 17 mA/cm^2.

The conclusion is the same as the result of the studies conducted so far on this sensing element by other authors, *i.e*., the sample showed good sensitivity only to ammonia vapor. Quantitative analysis revealed that the sensor exhibited a 42% sensitivity to ammonia (NH_3), whereas its responses to interfering gases such as ethanol (C_2H_5OH) and acetone

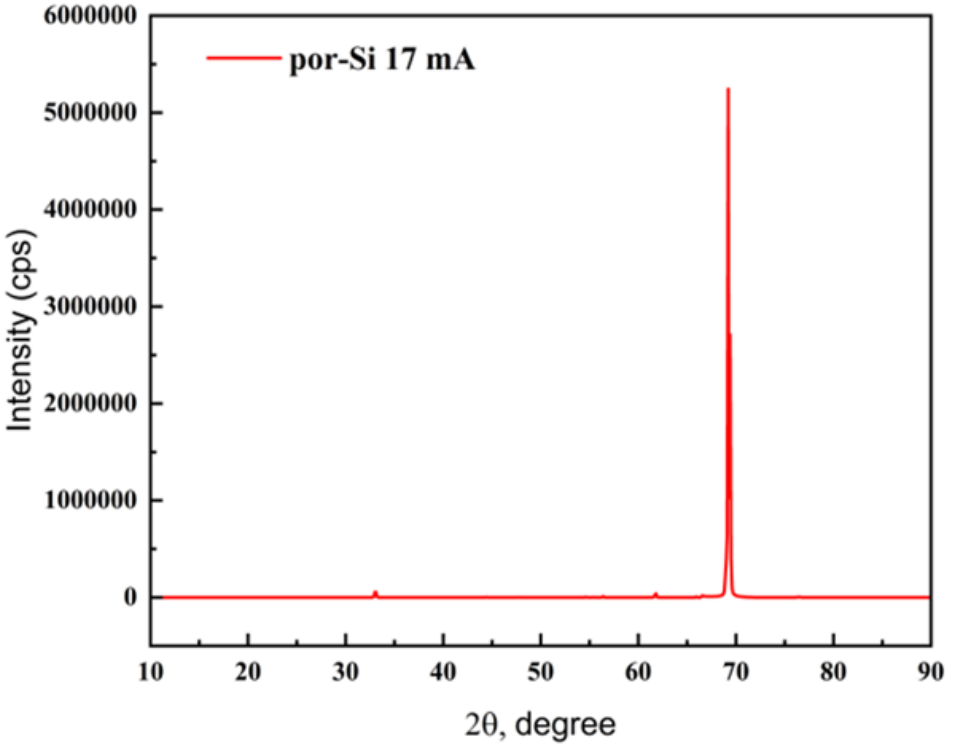

Fig. 9: XRD spectrum for PS sample etched at 17 mA/cm^2.

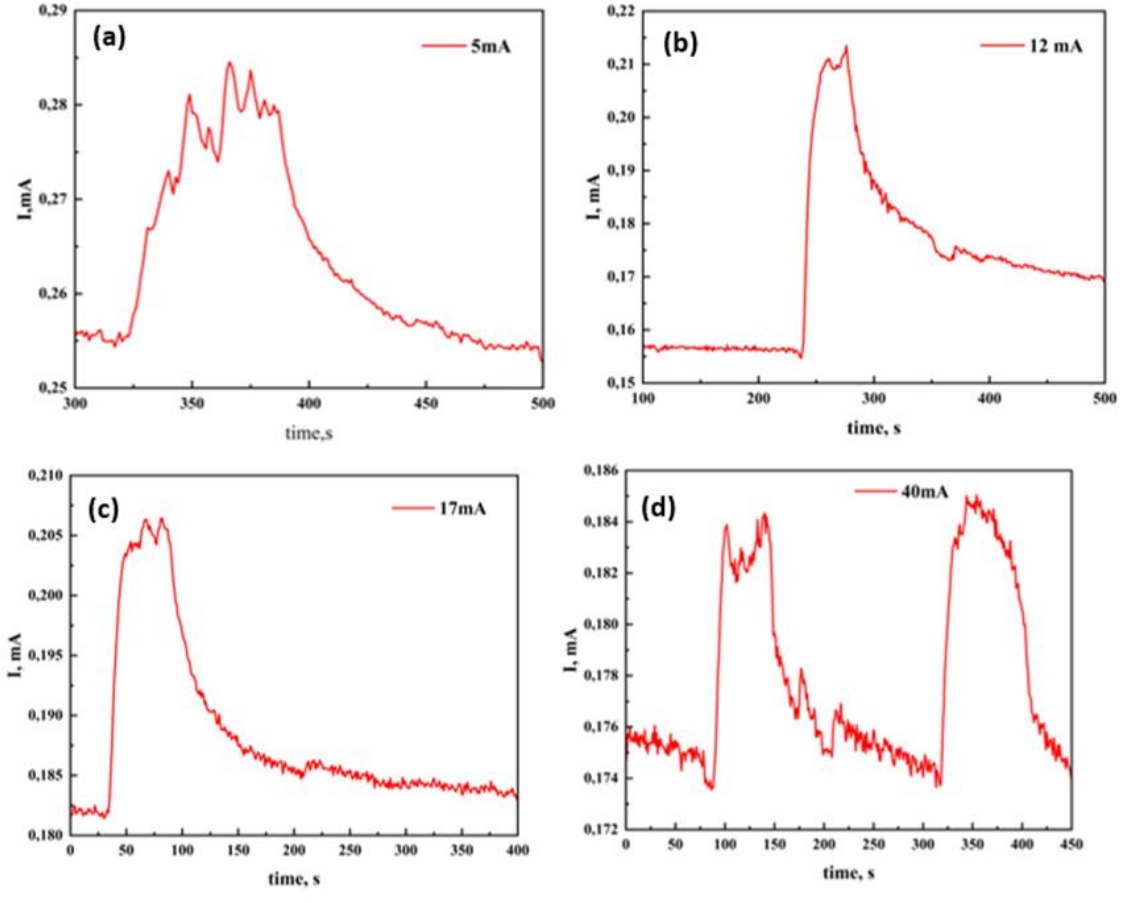

Fig. 10: Sensitivity and velocity of porous silicon samples when exposed to ammonia gas: a) 5 mA/cm^2; b) 12 mA/cm^2; c) 17 mA/cm^2; d) 40 mA/cm^2.

Table 2: Description of the production parameters of the sensor.

Sample	5 mA/ cm^2	12 mA/ cm^2	17 mA/ cm^2	40 mA/ cm^2
Current value in air, mA	0.255	0.15	0.182	0.174
Current value at interaction with gas, mA	0.285	0.213	0.206	0.184
Sensitivity, (%) ± Δ	12±1	42±3	13±1	6±5
Response time, (s) ± Δ	8±3	20±5	14±5	13±5
Recovery time, s	79	800	300	126

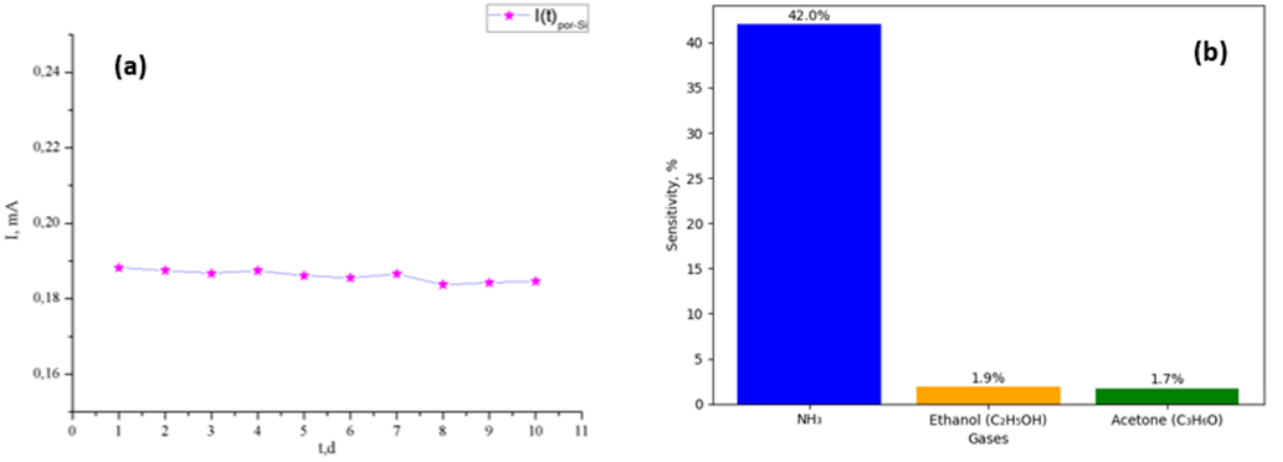

Fig. 11: Stability (a) and selectivity (b) of the PS-based gas sensor to gaseous ammonia vapor.

(C_3H_6O) were notably lower, amounting to 1.9% and 1.7%, respectively. Selectivity was determined by comparing the sensor sensitivity (S, %) to the target gas with its sensitivity to other interfering vapors under identical experimental conditions. The gas that produces the highest sensitivity under these controlled conditions is considered the most selectively detected by the sensor.

3.3 Fixed sensor data

The Blynk IoT platform was chosen to monitor the device's performance, which is ideal for such tasks. In this platform, a choice of ESP32 and Wi-Fi is available to create and configure the device.

Blynk provides three types of pins: virtual, digital, and analog. Virtual pins were chosen for this project because of their flexibility in customization and integration with the platform. The virtual pins were added to the sketch, allowing sensor data to be sent to the Blynk application.

The Blynk platform visualizes data from temperature, humidity, gas, and motion sensors. All this data is transmitted via Wi-Fi in real time. Virtual pins allow you to customize the units of measurement for displaying the data, such as °C, %, ppm or text strings.

In this way, the Blynk platform has provided a convenient tool for controlling and monitoring the device's performance by providing a clear display of data in the app.

4. Conclusion

This study successfully developed a portable ammonia gas sensor based on electrochemically etched porous silicon, optimizing performance through a comprehensive evaluation of selectivity, sensitivity, stability, and response speed. The porous silicon layers fabricated at a current density of 12 mA/cm² using a 1:2 HF: ethoxyethanol electrolyte exhibited superior sensitivity to ammonia, achieving 42%, which significantly outperformed responses to other test gases such as acetone and ethanol. This enhanced performance stems from the material's tailored nanostructure and increased surface reactivity. The integration of the porous silicon sensing element with an ESP32 microcontroller and wireless connectivity resulted in a practical, low-power device capable of room-temperature operation, eliminating the need for energy-intensive heating components. Housed in a 3D-printed PLA enclosure, the complete sensor system demonstrated a rapid 20-second response time and stable operation over a 10-day testing period, with real-time monitoring enabled through a custom IoT platform.

This work's significance extends beyond the laboratory, providing a practical pathway to translate porous silicon fabrication into functional sensing devices using accessible prototyping techniques such as CNC machining and 3D printing. The achievement of room-temperature operation combined with wireless functionality addresses critical

challenges in developing deployable gas monitoring solutions for environmental protection and industrial safety applications. This research represents an important step forward in creating smart, energy-efficient gas sensing systems that combine advanced nanomaterials with modern IoT capabilities for environmental monitoring and safety applications.

Acknowledgements
The authors gratefully acknowledge the financial support provided by the Ministry of Science and Higher Education of the Republic of Kazakhstan through Grant No. AP19678266. Additionally, they appreciate the support provided by the Targeted Program of the MHES of the Republic of Kazakhstan under Grant No. BR21882439.

Conflict of Interest
There is no conflict of interest.

Supporting Information
Not applicable.

CRediT Statement
Alisher Skabylov: Investigation, Data curation, Formal analysis, Visualization, Writing, original draft. **Lazzat Abdizhalilova:** Methodology, Investigation, Validation, Writing, review & editing. **Margulan Ibraimov:** Software, Formal analysis, Data curation, Visualization, Funding acquisition, Project administration. **Bakyt Khaniyev:** Resources, Investigation, Data curation. Yerbolat Tezekbay: Conceptualization, Methodology, Supervision, Funding acquisition, **Muhammad Abdullah:** Formal analysis, Writing, review & editing, Visualization. **Raikhan Azamat:** Resources, Supervision, Writing, review & editing. **Olzat Toktarbaiuly:** Conceptualization, Methodology, Supervision, Writing, review & editing. **Tolagay Duisebayev:** Conceptualization, Methodology, Project administration, Supervision**.** Writing, review & editing.

References
[1] S. Ozdemir, J. L. Gole, The potential of porous silicon gas sensors, *Current Opinion in Solid State and Materials Science*, 2007, **11**, 92-100, doi: 10.1016/j.cossms.2008.06.003.
[2] S. Zhu, X. Liu, J. Zhuang, L. Zhao, A fast room temperature NH_3 sensor based on an Al/p-Si/Al structure with Schottky electrodes, *Sensors*, 2017, **17**, 1929, doi: 10.3390/s17081929.
[3] Y. Li, G. Feng, X. Liu, H. Li, B. Dong, L. Zhao, Enhanced ammonia gas sensing response of Al-hyperdoped black silicon sensor at room temperature, *Chinese Journal of Physics*, 2025, **93**, 381-388, doi: 10.1016/j.cjph.2024.12.013.
[4] V. Usov, S. Stoyanov, C. O Coileain, O. Toktarbaiuly, I. V. Shvets, Antiband instability on vicinal Si(111) under the condition of diffusion-limited sublimation, *Physical Review B*, 2012, **86**, 195317, doi: 10.1103/physrevb.86.195317.
[5] V. Usov, C. Ó. Coileáin, A. N. Chaika, S. I. Bozhko, V. N. Semenov, S. Krasnikov, O. Toktarbaiuly, S. Stoyanov, I. V. Shvets, Revealing electromigration on dielectrics and metals through the step-bunching instability, *Physical Review B*, 2020, **102**, 035407, doi: 10.1103/physrevb.102.035407.
[6] M. Verma, G. Bahuguna, S. Singh, A. Kumari, D. Ghosh, H. Haick, R. Gupta, Porous SnO_2 nanosheets for room temperature ammonia sensing in extreme humidity, *Materials Horizons*, 2024, **11**, 184-195, doi: 10.1039/D3MH01078C.
[7] J. C. Santos-Ceballos, F. Salehnia, F. Güell, A. Romero, X. Vilanova, E. Llobet, Room-temperature ammonia sensing using polyaniline-coated laser-induced graphene, *Sensors*, 2024, **24**, 7832, doi: 10.3390/s24237832.
[8] Y. Shang, X. Wang, E. Xu, C. Tong, J. Wu, Optical ammonia gas sensor based on a porous silicon rugate filter coated with polymer-supported dye, *Analytica Chimica Acta*, 2011, **685**, 58-64, doi: 10.1016/j.aca.2010.11.008.
[9] Y. Vashpanov, J. I. Jung, K. D. Kwack, Photo-EMF sensitivity of porous silicon thin layer-crystalline silicon heterojunction to ammonia adsorption, *Sensors*, 2011, **11**, 1321-1327, doi: 10.3390/s110201321.
[10] E. Afsharmanesh, H. Haratizadeh, F. Bagheri, Self-powered highly selective and fast response time ammonia gas sensors based on an rGO/SnO_2 nanocomposite, *Sensors and Actuators A: Physical*, 2024, **379**, 115963, doi: 10.1016/j.sna.2024.1159
[11] H. R. Abed, A. M. Alwan, A. A. Yousif, N. F. Habubi, Efficient SnO_2/CuO/porous silicon nanocomposites structure for NH_3 gas sensing by incorporating CuO nanoparticles, *Optical and Quantum Electronics*, 2019, **51**, 333, doi: 10.1007/s11082-019-2046-y.
[12] R. Hossain, K. Hassan, V. Sahajwalla, Utilising problematic waste to detect toxic gas release in the environment: fabricating a NiO doped CuO nanoflake based ammonia sensor from e-waste, *Nanoscale Advances*, 2022, **4**, 4066-4079, doi: 10.1039/D1NA00743B.
[13] M. J. Saadh, A. Basem, Z. A. Hanoon, M. Al-Bahrani, J. Mgm, J. C. Jie, K. Muzammil, M. A. Hasan, S. Islam, R. Zainul, Adsorption of NH_3, HCHO, SO_2, and Cl_2 gasses on the o-B2N2 monolayer for its potential application as a sensor, *Diamond and Related Materials*, 2024, **147**, 111356, doi: 10.1016/j.diamond.2024.111356.
[14] Y. Seekaew, W. Pon-On, C. Wongchoosuk, Ultrahigh selective room-temperature ammonia gas sensor based on tin-titanium dioxide/reduced graphene/carbon nanotube nanocomposites by the solvothermal method, *ACS Omega*, 2019, **4**, 16916-16924, doi: 10.1021/acsomega.9b02185.
[15] R. Gao, X. Ma, L. Liu, S. Gao, X. Zhang, Y. Xu, X. Cheng, H. Zhao, L. Huo, In-situ, deposition of POMA/ZnO nanorods array film by vapor phase polymerization for detection of trace

ammonia in human exhaled breath at room temperature, *Analytica Chimica Acta*, 2022, **1199**, 339563, doi: 10.1016/j.aca.2022.339563.

[16] O. Toktarbaiuly, Enhancement of power conversion efficiency of dye-sensitized solar cells *via* incorporation of Gan semiconductor material synthesized in hot-wall chemical vapor deposition furnace, *Eurasian Physical Technical Journal*, 2024, **21**, 131-139, doi: 10.31489/2024no4/131-139.

[17] Y. Zhuang, X. Wang, P. Lai, J. Li, L. Chen, Y. Lin, F. Wang, Wireless flexible system for highly sensitive ammonia detection based on polyaniline/carbon nanotubes, *Biosensors*, 2024, **14**, 191, doi: 10.3390/bios14040191.

[18] C. Li, B. Li, G. Shi, Design of electronic remote control system based on wireless sensor, *International Journal of Online and Biomedical Engineering (IJOE)*, 2017, **13**, 146-159, doi: 10.3991/ijoe.v13i05.7057.

[19] S. B. Shahewaz, C. R. Prasad, Gas leakage detection and alerting system using Arduino Uno, *Global Journal of Engineering and Technology Advances*, 2020, **5**, 29-35, doi: 10.30574/gjeta.2020.5.3.0109.

[20] A. Coboi, M. T. Nguyen, K. T. La, T. C. Vu, Wireless sensor network based gas monitoring system utilizing ZigBee technology, *Journal of Electronics and Electrical Engineering*, 2023, **2**, 190-207, doi: 10.37256/jeee.2220233418.

[21] J.-H. Suh, I. Cho, K. Kang, S.-J. Kweon, M. Lee, H.-J. Yoo, I. Park, Fully integrated and portable semiconductor-type multi-gas sensing module for IoT applications, *Sensors and Actuators B: Chemical*, 2018, **265**, 660-667, doi: 10.1016/j.snb.2018.03.099.

[22] P. Arroyo, F. Meléndez, J. I. Suárez, J. L. Herrero, S. Rodríguez, J. Lozano, Electronic nose with digital gas sensors connected *via* bluetooth to a smartphone for air quality measurements, *Sensors*, 2020, **20**, 786, doi: 10.3390/s20030786.

[23] A. Zompanti, M. Santonico, L. Vollero, S. Grasso, A. Sabatini, F. Mereu, A. D'Amico, G. Pennazza, A gas sensor with BLE connectivity for wearable applications, *EUROSENSORS* MDPI, 2018, **2**(13), 765, doi: 10.3390/proceedings2130765.

[24] J.-C. Chiou, C.-C. Wu, A wearable and wireless gas-sensing system using flexible polymer/multi-walled carbon nanotube composite films, *Polymers*, 2017, **9**, 457, doi: 10.3390/polym9090457.

[25] B. A. Khaniyev, Y. Sagidolda, K. K. Dikhanbayev, A. O. Tileu, M. K. Ibraimov, High sensitive NH_3 sensor based on electrochemically etched porous silicon, *Cogent Engineering*, 2020, **7**, 1810880, doi: 10.1080/23311916.2020.1810880.

[26] M. H. Kareem, A. M. Abdul Hussein, H. T. Hussein, Preparation high quality ethanol gas sensor by modifying porous silicon (PS) surface with carbon nanotube (CNTs), *Optik*, 2022, **259**, 168826, doi: 10.1016/j.ijleo.2022.168826.

[27] L. Huo, X. Yang, Z. Liu, X. Tian, T. Qi, X. Wang, K. Yu, J. Sun, M. Fan, Modulation of potential barrier heights in Co_3O_4/SnO_2 heterojunctions for highly H2-selective sensors, *Sensors and Actuators B: Chemical*, 2017, **244**, 694-700, doi: 10.1016/j.snb.2017.01.061.

[28] N. Sharma, S. P. Choudhury, Gas sensing using metal oxide semiconductor doped with rare earth elements: a review, *Materials Science and Engineering: B*, 2024, **307**, 117505, doi: 10.1016/j.mseb.2024.117505.

[29] N. Baran, H. Gebavi, L. Mikac, D. Ristić, M. Gotić, K. A. Syed, M. Ivanda, Sensing properties of oxidized nanostructured silicon surface on vaporized molecules, *Sensors*, 2019, **19**(1), 119, doi: 10.3390/s19010119.

[30] H. Chai, Z. Zheng, K. Liu, J. Xu, K. Wu, Y. Luo, H. Liao, M. Debliquy, C. Zhang, Stability of metal oxide semiconductor gas sensors: a review, *IEEE Sensors Journal*, 2022, **22**, 5470-5481, doi: 10.1109/JSEN.2022.3148264.

[31] A. Koushal, R. Gupta, F. Jan, K. Kamaldeep and V. Kumar, "Home Automation System Using ESP32 and Firebase," 2022 *Seventh International Conference on Parallel, Distributed and Grid Computing (PDGC)*, Solan, Himachal Pradesh, India, 2022, 228-231, doi: 10.1109/PDGC56933.2022.10053309.

[32] G. P. N. Hakim, M. H. I. Hajar, A. Firdausi, E. Ramadhan, Benchmarking in microcontroller development board power consumption for low power iot wsn application, *Jurnal Teknologi Elektro*, 2022, **13**, 25, doi: 10.22441/jte.2022.v13i1.005.

[33] A. Maier, A. Sharp and Y. Vagapov, "Comparative analysis and practical implementation of the ESP32 microcontroller module for the internet of things," *2017 Internet Technologies and Applications (ITA)*, Wrexham, UK, 2017, 143-148, doi: 10.1109/ITECHA.2017.8101926.

[34] S. Buakaew, A. Ausama, N. Atiwongsangthong, Ambient gases sensing by photoluminescence properties of porous silicon, *8th International Conference on Engineering, Applied Sciences, and Technology (ICEAST)*. June 8-10, 2022, Chiang Mai, Thailand. IEEE, 50-53, doi: 10.1109/ICEAST55249.2022.9826322.

[35] Y. Li, G. Feng, X. Liu, H. Li, B. Dong, L. Zhao, Enhanced ammonia gas sensing response of Al-hyperdoped black silicon sensor at room temperature, *Chinese Journal of Physics*, 2025, **93**, 381-388, doi: 10.1016/j.cjph.2024.12.013.